Attosecond Delays in X-ray Molecular Ionization

Taran Driver[1,2*], Miles Mountney[3], Jun Wang[1,2,4], Lisa Ortmann[5], Andre Al-Haddad[6], Nora Berrah[7], Christoph Bostedt[6,8], Elio G. Champenois[1], Louis F. DiMauro[5], Joseph Duris[9], Douglas Garratt[13], James M. Glownia[2], Zhaoheng Guo[4,9], Daniel Haxton[10], Erik Isele[1,2,4], Igor Ivanov[11], Jiabao Ji[12], Andrei Kamalov[1], Siqi Li[9], Ming-Fu Lin[2], Jon P. Marangos[13], Razib Obaid[7], Jordan T. O'Neal[1], Philipp Rosenberger[14,15], Niranjan H. Shivaram[2,17], Anna L. Wang[1], Peter Walter[2], Thomas J. A. Wolf[1,2], Hans Jakob Wörner[12], Zhen Zhang[9], Philip H. Bucksbaum[1,4], Matthias F. Kling[1,2,14,15], Alexandra S. Landsman[5], Robert R. Lucchese[16], Agapi Emmanouilidou[3], Agostino Marinelli[1,9*], James P. Cryan[1,2*]

[1]Stanford Pulse Institute, SLAC National Accelerator Laboratory, Menlo Park, California, USA.

[2]Linac Coherent Light Source, SLAC National Accelerator Laboratory, Menlo Park, California, USA.

[3]Department of Physics and Astronomy, University College London, London, , United Kingdom.

[4]Applied Physics Department, Stanford University, Stanford, California, USA.

[5]Department of Physics, The Ohio State University, Columbus, Ohio, USA.

[6]Paul Scherrer Institute, Villigen, Switzerland.

[7]Department of Physics, University of Connecticut, Storrs, Connecticut, USA.

[8]LUXS Laboratory for Ultrafast X-ray Sciences, Institute of Chemical Sciences and Engineering, Ecole Polytechnique Federale de Lausanne (EPFL), Lausanne, Switzerland.

[9]SLAC National Accelerator Laboratory, Menlo Park, California, USA.

[10]KLA Corporation, Milpitas, California, USA.

[11]Center for Relativistic Laser Science, Institute for Basic Science, Gwangju, Korea.

[12]Laboratorium fur Physikalische Chemie, ETH Zurich, Zurich, Switzerland.
[13]The Blackett Laboratory, Imperial College London, London, United Kingdom.
[14]Physics Department, Ludwig-Maximilians-Universitat, Munich, Germany.
[15]Max Planck Institute of Quantum Optics, Garching, Germany.
[16]Chemical Sciences Division, Lawerence Berkeley National Laboratory, Berkeley, California, USA.
[17]Department of Physics and Astronomy and Purdue Quantum Science and Engineering Institute, Purdue University, West Lafayette, Indiana, USA.

*Corresponding author(s). E-mail(s): tdriver@stanford.edu; marinelli@slac.stanford.edu; jcryan@slac.stanford.edu;
Contributing authors: landsman.7@osu.edu; rlucchese@lbl.gov; a.emmanouilidou@ucl.ac.uk;

Abstract

The photoelectric effect is not truly instantaneous, but exhibits attosecond delays that can reveal complex molecular dynamics. Sub-femtosecond duration light pulses provide the requisite tools to resolve the dynamics of photoionization. Accordingly, the past decade has produced a large volume of work on photoionization delays following single photon absorption of an extreme ultraviolet (XUV) photon. However, the measurement of time-resolved core-level photoionization remained out of reach. The required x-ray photon energies needed for core-level photoionization were not available with attosecond tabletop sources. We have now measured the x-ray photoemission delay of core-level electrons, and here report unexpectedly large delays, ranging up to 700 attoseconds in NO near the oxygen K-shell threshold. These measurements exploit attosecond soft x-ray pulses from a free-electron laser (XFEL) to scan across the entire region near the K-shell threshold. Furthermore, we find the delay spectrum is richly modulated, suggesting several contributions including transient trapping of the photoelectron due to shape resonances, collisions with the Auger-Meitner electron that is emitted in the rapid non-radiative relaxation of the molecule, and multi-electron scattering effects. The results demonstrate how x-ray attosecond experiments, supported by comprehensive theoretical modelling, can unravel the complex correlated dynamics of core-level photoionization.

Keywords: ultrafast, attosecond, x-ray free electron laser, photoionization delay

Introduction

Understanding complex multi-electron interactions is a frontier scientific challenge since electron-electron interactions (or correlations) play a fundamental role in determining the properties of matter. The photoelectric effect (or photoionization) in isolated atoms or molecules is inherently a multi-electron process. Even if only one electron is removed from a molecule, the electronic wavefunction of the residual ion will rearrange during and after the interaction with the ionizing field. This effect is especially pronounced when the electron is removed from a core-level orbital of a molecular system.

In this work, we use attosecond x-ray pulses to measure the temporal retardation of photoemission between electrons emitted from the oxygen and nitrogen K-shells of nitric oxide.The photoelectric effect was long treated as an instantaneous process, because the extreme timescales associated with photoionization dynamics were inaccessible to experimental science. However, the development of attosecond duration light pulses, has made it possible to achieve the requisite time resolution to resolve the dynamics of photoionization [1, 2]. Time-domain measurements of photoemission have provided rich information on electron correlation effects in the system being ionized [3–12], which is inaccessible to other electronic observables, such as electron binding energy, partial-photoionization cross-section, or photoelectron angular distribution. The photoemission time delay can be related to the kinetic energy dispersion of the phase of the dipole matrix element for x-ray photoionization [13], which enables the complete measurement (amplitude and phase) of a fundamental quantum phenomenon, the photoelectric effect. Moreover, we find that the inclusion of electron correlation effects are critical for accurately modeling our experimental results.In doing so, we demonstrate that K-shell photoemission delays offer a sensitive experimental probe of correlated electron motion in multi-electron systems.

Previous measurements of photoemission delays has employed methods such as RABBITT [14–16] and laser streaking [1, 17]. Initially used to study photoemission processes in atoms ~~[1, 16, 18]~~[1, 16, 18, 19], these techniques have also been extended to molecular systems [6, 7, 10, 20–23]. These studies have lead to a deeper understanding of photoionization, particularly ionization in the vicinity of continuum structures [3–12, 20–23]. ~~To date, a significant limitation of these measurements has been the sparsity at which the electron kinetic-energy-dependent photoionization delay can be probed. In typical experiments only a few (3-5) kinetic energy points can be collected, and this limits the ability to compare these results with theory. However with the~~ With the advent of tunable attosecond-XFEL sources [24], it is now possible to tune continuously across a large range of electron kinetic energies. To this end, we employ attosecond angular streaking [24–28] using x-ray pulses from a free-electron laser to extend measurements of photoemission time-delays to core-level (K-shell) electrons.

Attosecond angular streaking

In angular streaking an ionizing attosecond x-ray pulse is overlapped with a circularly-polarized, long wavelength (infrared) laser field. The infrared (IR) dressing field maps

the temporal profile of the x-ray photoemission to the final momentum of the photoelectrons.This mapping is similar to the principle of a time-resolving streak camera [29] and takes place *via* the so-called streaking interaction [17, 30]. In a semi-classical approximation, the final momentum of an ionized electron measured at a detector is described (in atomic units) by

$$\vec{p}(t \to \infty) = \vec{p}_0 + e\vec{A}(t_0), \tag{1}$$

where $\vec{A}(t_0) = -\int_{-\infty}^{t_0} \vec{\mathcal{E}}_L(t')dt'$ is the vector potential of the circularly polarized laser field, $\mathcal{E}_L(t)$, the time, t_0, the electron is released into the continuum, e is the charge of an electron and $\vec{p}_0$ is the momentum of the electron in the absence of the IR field. In this semi-classical approximation, the interaction with the laser maps the arrival time of the x-ray pulse to the angle of the electron momentum shift (or streaking angle). In the presence of a short-range potential, the interaction between the outgoing electron and the potential modifies the streaking angle, and the apparent emission time of the electron is effectively delayed with respect to the arrival time of the ionizing pulse. This delay can be attributed to the group velocity of the outgoing electronic wavepacket [1], as shown in the supporting material, and can be related to the kinetic energy dispersion of the phase of the photoionization matrix elements [13].

To define a delay, we must specify a reference event. We measure the photoemission delay of low energy electrons from the oxygen K-shell of nitric oxide with respect to >120 eV electrons emitted from the nitrogen K-shell of the same molecule ionzied by the same attosecond x-ray pulse. The photoemission delay of the high-energy nitrogen K-shell electrons is not strongly affected by correlation effects and can be calculated with confidence to be less than ~ 5 as with reference to the arrival of the x-ray pulse [13, 18, 31]. The photon energy ~~was scanned in 0.5 eV steps of~~ the x-ray pulse was scanned across the oxygen ~~K-edge~~ near-edge ~~X-ray absorption fine structure (NEXAFS)~~ region ($540-580$ eV) while measuring the momentum shift experienced by the oxygen and nitrogen K-shell electrons.

Our measurement was performed at the Atomic, Molecular and Optical physics (AMO) experimental hutch at the Linac Coherent Light Source (LCLS), using attosecond x-ray pulses produced by enhanced self-amplified spontaneous emission (ESASE) [24, 28, 32]. Photoelectrons produced by X-ray ionization were streaked by combining attosecond x-ray pulses with a co-propagating 2.3 μm wavelength, circularly polarized laser pulse with ~ 100 fs FWHM duration. The momentum distribution of the emitted photoelectrons was recorded using a co-axial velocity map imaging (c-VMI) spectrometer, as shown in Fig. 1, which was designed for measurement of high energy electrons [28, 33].

The vector potential of the circularly polarized streaking pulse rotates with angular velocity $2\pi/T$, where $T_L = 7.7$ fs for a wavelength of 2.3 μm. Therefore the difference in momentum shift $-\vec{A}(t_i)$ between different photoelectron features produced by the same x-ray pulse encodes the delay between the two photoemission events [28]. Because the period T_L of the circularly polarized laser was well-known in our experiment, if the momentum shift between two photoelectron features is $\Delta\theta$, the photoemission events

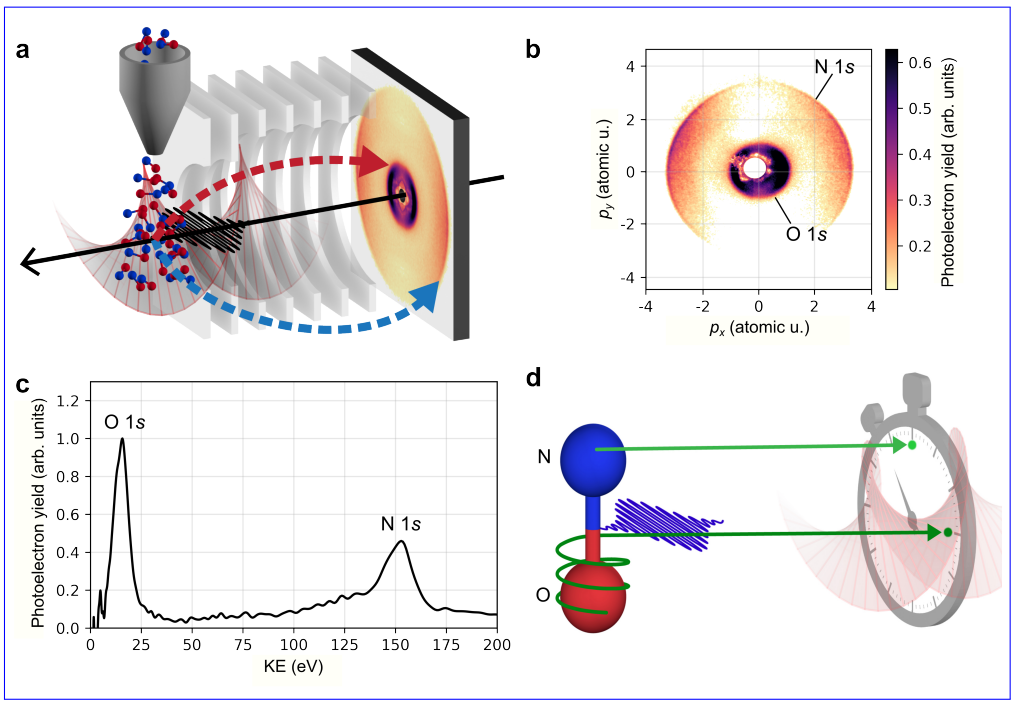

Fig. 1 **a** Experimental setup showing electrons ionized by the x-ray pulse (~~purple~~black) from the nitrogen (blue) and oxygen (red) K-shells incident on the detector of the cVMI [33] spectrometer. **b** Momentum distribution of photoelectrons in the absence of the streaking field at an x-ray central photon energy of 563 eV. **c** Kinetic energy distribution by inverse Abel transformation of momentum distribution in panel **b**. **d** Electrons ionized from the nitrogen and oxygen K-shells, respectively, experience different trajectories in the molecular potential, resulting in a relative photoemission delay. (see text for details)

were separated by a time $\Delta\tau$:

$$\Delta\tau = \frac{\Delta\theta}{2\pi} \times T_L. \tag{2}$$

The momentum shift can be seen in the data plotted in Figure 2, which shows the differential electron momentum distribution measured for 552 eV x-rays in Cartesian (a) and polar (b) coordinates. The electron momentum distribution is plotted as a difference image between measurements where the direction of vector potential of the IR laser at the time when the x-ray pulse ~~ionizied~~ ionized the sample made a ~~170°~~ 180° angle with respect to the x-ray polarization (the long arrow in panel (a) and the dashed-red line in panel(b)) and measurements where the IR laser was intentionally mistimed with respect to the x-ray pulse. The momentum shift of the electrons ionized from the nitrogen K-shell (high energy feature) is in the direction of the IR vector potential at the time of ionization. It is clear for panels (a) and (b) that the momentum shift of the lower energy, oxygen K-shell ionization feature, is different, implying a delay in the emission of the oxygen K-shell electrons.

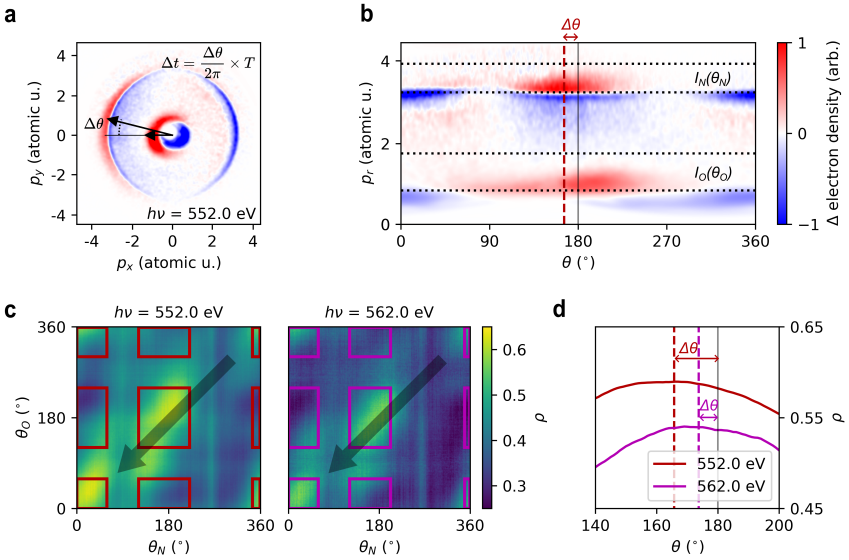

Fig. 2 **a** Differential photoelectron momentum distribution (see text) induced by the IR streaking laser for only one x-ray/laser arrival time. The relative photoemission delay is proportional to the difference in angle $\Delta\theta$ between the momentum shift of the oxygen and nitrogen photolines. This distribution is rebinned to polar coordinates in panel **b**, and the vectors $I_N(\theta_N)$ and $I_O(\theta_O)$ are defined by integrating the labeled regions along the radial coordinate. **c** Partial correlation maps recorded at two different photon energies. The marked regions of the maps are averaged in the direction indicated by the black arrows to produce the traces shown in panel **d**. The offset of the position of maximum correlation gives the angular difference in momentum shift between the two photoelectron distributions.

Data Analysis

To measure the differential direction of the momentum shift between the high energy electrons ionized from the nitrogen K-shell (N1s) and the low energy electrons ionized from the oxygen K-shell (O1s) and extract the relative photoemission delay using Eqn. 2, we exploit the inherent temporal jitter between the x-ray pulse and the circularly polarized laser (~ 500 fs full-width-at-half-maximum (FWHM) [34]). The scheme is illustrated in the lower panels of Fig. 2. The temporal jitter between the x-rays and the streaking field results in shot-to-shot variation ~~the in~~ in the momentum shift of the oxygen and nitrogen K-shell photoemission features, but the difference between these two angles remains fixed. This difference can be isolated in the partial correlation map (defined in the methods section) between the angle-resolved electron yield in two different regions of our detector. These regions correspond to the high kinetic energy side of the N1s and O1s photoemission features respectively, as shown in panel **b** of Fig. 2. Calculating the partial correlation removes the spurious correlation due to shot-to-shot fluctuations in the FEL, pulse energy, spectrum, etc. The angular difference between the momentum shift of the two features is encoded in the offset between the peak of the partial correlation coefficient from the diagonal of this map, shown

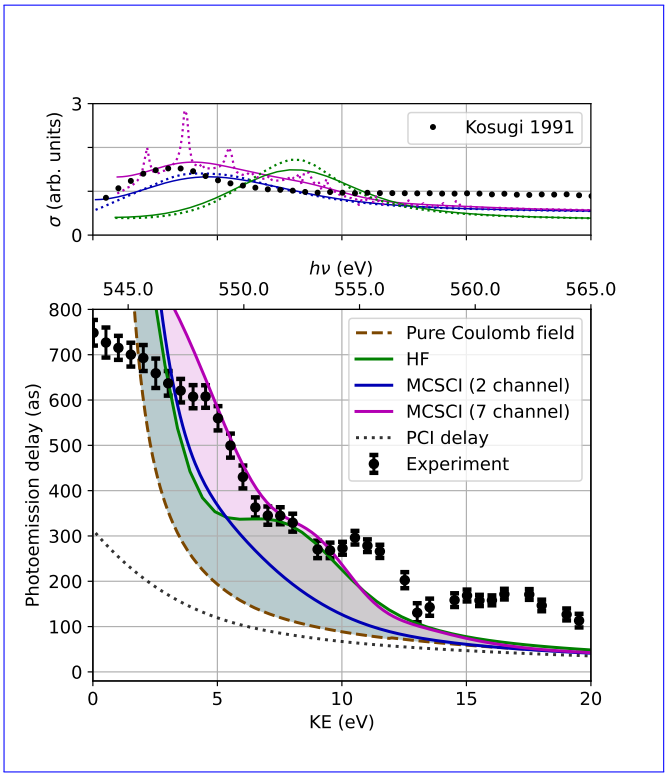

Fig. 3 Oxygen K-shell photoionization cross-section (upper panel) in the Hartree Fock approximation (green), two-channel (blue), and seven-channel (magenta) Schwinger configuration interaction method. The calculated result is shown as a ~~dashed~~ dotted curve, and the solid curve shows the results convoluted with the expected photon energy distribution from the XFEL. The black ~~dashed~~ dotted line shows the photoabsorption cross-section measured by Kosugi *et al.* [35]. The experimental photoemission delay (black points) is shown in the lower panel along with calculated photoemission delay. The contribution to the delay from the post-collision interaction (PCI) is also shown (dotted black line).

in panel **c** of Fig. 2. This analysis is further described in the Supplementary Information (SI). The measured kinetic energy-dependent photoemission delay between the O1s and N1s photoelectrons is shown in Fig. 3.

The photoelectron spectrum shown in Fig. 1 (c) contains two features, one corresponding to an ionization which leaves the residual cation in a $^3\Sigma$ state and another where the residual cation is found to be in a $^1\Sigma$ state. The binding energy difference between these two features is ~ 0.7 eV (543.3 eV/544 eV, respectively [35]) and is not resolved in this experiment. Thus the experimental data presented in Fig. 3 is a mixture of both ionization channels taking into account that the $^3\Sigma$-channel has a roughly three-fold higher cross-section [36].

Discussion

The measured photoemission delay of the low energy electrons from the oxygen K-shell (black points in Fig. 3) decreases with increasing kinetic energy, as expected. The

group delay incurred by a photoelectron wavepacket in a ~~simple~~ Coulomb potential is given by the derivative of the ~~argument of the~~ Coulomb phase-shift, $\partial_E \sigma_l$, where, $\sigma_l = \arg[\Gamma(l+1-\frac{iZ}{k})]$, l is the angular momentum of the photoelectron, Z is the charge of the residual ion and $k^2/2$ is the kinetic energy of the photoelectron. This simple analytical form (plotted in dashed brown in Fig. 3) accounts for the expected photoemission delay ~~from a centrosymmetric system, such as an atom.~~ for an electron emerging from a pure Coulomb field, i.e. ionization of a hydrogenic system. There is an additional contribution to the extracted photoemission delay due to fact that the photoelectron is being driven by the streaking laser field in the presence of the long-range Coulomb potential of the ion. This so-called Coulomb laser coupling (CLC) delay was calculated for the case of circular polarization using the classical trajectory Monte Carlo (CTMC) method, which is described further in the SI, and ~~then subtracted from the pure Coulomb delay~~ opposes the delay from the Coulomb field. The curves in Fig. 3 ~~.~~ are a summation of this CLC contribution and the pure Coulomb delay.These purely Coulombic effects describe the general trend of the measured photoemission delay, i.e. a decreasing delay with increasing photoelectron kinetic energy, however the absolute agreement is poor, pointing to the importance of molecular structure in the attosecond delay dispersion.

To understand our measured delay, we compare with numerical calculations of photoionization of the oxygen K-shell of nitric oxide. We initially employ a single center expansion (SCE) for the continuum wavefunction, solving a system of Hartree-Fock (HF) equations [37]. The bound states of the core-excited NO^{+*} ion are computed using the HF method with the *aug-cc-pVQZ* basis set. We choose to use the bound states of the core-excited NO^{+*} ion to better approximate the orbital contraction that occurs during ionization. Using these states we calculate the photoionization matrix element (PME) in the dipole approximation. From the PME, we can calculate the orientation- and electron emission direction-resolved cross-section and delay, as described in the methods [38]. The calculation of the photoemission delay is then convolved with a gaussian kernel of width $\sigma = 1.3$ eV to account for the inherent spectral jitter in the XFEL photon energy [24, 28]. The green curves in Fig. 3 show the calculated delay (and cross-section in the upper panel).At the HF level of electronic structure theory, the calculated photoemission delay (green curve) is much closer to the measured delay, compared to the ~~atomic~~ delay for a pure Coulomb potential theory (dashed brown curve).

For a molecular system, the photoemission delay maps to molecular effects arising from the complex shape of the potential of the residual molecular ion [6, 7, 21]. In the case of K-shell ionization of nitric oxide, there is ~~noted~~ noticeable increase in the photoionization cross-section ~ 4 eV above the K-shell threshold, as shown by the measurements of Kosugi *et al.* [35] reproduced in the upper panel of Fig. 3. This increase has been postulated to result from the existence of a shape resonance in the electronic continuum. The shape resonance occurs when the outgoing photoelectron experiences a transient trapping due to a combination of the molecular potential and the centrifugal barrier created by the photoelectron angular momentum [39]. The electron can tunnel through the barrier and leave the molecular potential, resulting in an increase in the photoemission time delay.

The HF calculation shows a similar increase in the photoionization cross-section above the K-shell threshold, although the energetic position of the maximum in the cross-section is shifted by several electron volts compared to the measurement. Turning to the calculated photoemission delay, we can see that this increase in cross-section coincides with an increase in the calculated photoemission delay, which is indicative of a molecular shape resonance.

It is worth noting that the shape resonance only appears in the HF calculation when we use the core-excited NO^{+*} bound states ~~in the HF calculation the~~ to solve for the continuum wavefunction [37, 40]. Using the bound states from the neutral NO molecule fails to produce a shape resonance in the continuum. In contrast ~~the~~ to valence ionization, which creates a delocalized hole in the electronic density of the molecule, ionization of a highly-localized core-level causes the electron density in the ion to contract around the core-level vacancy, a consequence of the highly correlated nature of the core-level electrons [40–42]. By using pre-contracted orbitals in the calculation we can approximate the correlation interaction of the core-level electrons even though we perform a mean field calculation.

While the HF calculation is able to explain some of the structure in the photoemission delay, the theory fails to reproduce the entire measurement. In an attempt to better describe the delays we calculate the photoionization matrix element using the multichannel Schwinger configuration interaction (MCSCI) method. The orientation- and electron emission direction-resolved cross-section and delay for two channels ($^1\Sigma$ and $^3\Sigma$) and seven channels ($^1\Sigma$, $^3\Sigma$, and five additional shake-up states) are shown as the blue and purple curves in Fig. 3, respectively. Again these results have been convolved with the same gaussian kernel to account for the jitter in the XFEL photon energy. Both the two-channel and seven-channel calculations predict a shape resonance just above the K-shell threshold, which results in an increase in the photoionization cross-section consistent with the previous measurements. However, the expected increase in the photoionziation delay due to the presence of the shape resonance is less pronounced in the two-channel calculation (compared to the HF calculation). This is a result of the shape resonance shifting to lower kinetic energy, where the Coulomb contribution to the photoemission delay is much larger. Thus, the two-channel calculation provides an improvement over the HF calculation in the description of the photoionizaiton cross-section, but does not significantly alter the agreement between the measured and calculated photoemission time delay.

Turning our attention to the seven-channel model, the photoionization cross-section (dashed magneta line) in the top panel of Fig. 3 shows a series of sharp autoionizing shake-up features, in addition to a shape resonance. While these features appear quite distinct, once the calculation is averaged over several N-O bond lengths (which shifts ~~their energetic position~~ the energetic position of the resonant features, see SM) and convolved with the expected bandwidth and energy jitter of the XFEL, the cross-section again appears smooth (solid curves in upper panel of Fig. 3). There is however a marked effect on the photoemission delay, which increases significantly between the two-channel and seven-channel calculation (purple shaded area in Fig. 3). The seven-channel calculation greatly improves the agreement with the measured photoemission delay. It is striking that the x-ray photoemission delay is strongly

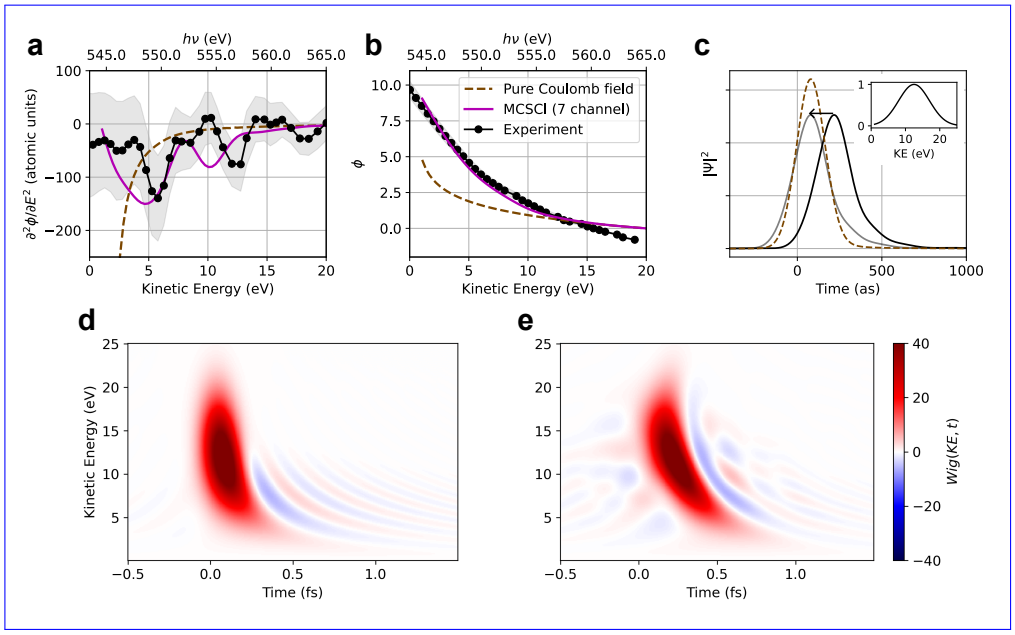

Fig. 4 First derivative with respect to energy (a) and integral (b) of the photoemission delays from Fig. 3(b). The black curve is derived from the measured data and the shaded gray area shows the standard error. The dashed brown curve shows the result calculated for ~~an atomic potential~~ a pure Coulomb field and the magenta curve shows the result from the 7-channel MCSCI calculation. The reshaping of the ~~photoionizied~~ photoionized wavepacket due to the molecular potential is shown in panels (c)-(e). Panel (d) shows the Wigner quasi-probability distribution of the ~~photoionizied~~ photoionized wavepacket in ~~the atomic~~ a pure Coulomb potential, and panel (e) shows the wavepacket reconstructed from the experimental phase shown in panel (b). The marginals (or projection) of the Wigner distribution along the energy axis are shown in panel (c)~~.~~. The dashed brown curve in the main panel shows the wavepacket from ~~an atomic potential~~a pure Coulombpotential. The black curve shows the result from the experimental phase. To illustrate the reshaping, we also show the ~~dashed black curve is the~~ experimental curve shifted to overlap with the centroid of the ~~atomic~~ pure Coulomb wavepacket (gray curve). The inset in panel (c) shows the marginal along the time-axis, which shows the spectral content of the electronic wavepacket.

dependent on channel-coupling in the final ionic state, demonstrating the sensitivity of x-ray photoemission delay for probing electron correlation effects. Our measurements confirm that the increase in photoioniztion cross-section just above the oxygen K-shell threshold is due to the combination of resonant features in the continuum, both a shape resonance, and unresolved autoionizing states.

For electrons with less than ~ 3 eV kinetic energy, we expect the separability of the photoionization delay and the CLC contribution to break down. The disagreement between our measurement and the calculation at higher electron kinetic energies is likely the result of additional ionization channels, not considered in the MCSCI calculation. For example, in a previous measurement of the symmetry-resolved ionization cross-section, Kosugi *et al.* [35] observed an increase in the ionization asymmetry parameter near an electron kinetic energy of ~ 17 eV, possibly indicating additional structure in the ionization continuum.

By employing a fully tunable attosecond XFEL, we have mapped out the photoemission delay in 0.5 eV steps between the K-shell ionization threshold (543 eV) and 565 eV. This is unique in photoemission delay measurements, which are usually performed at a fixed photon energy. This enhanced fidelity allows us to make better comparison with theory, as we can derive other observables from the measurement. For instance, Fig. 4 (a) shows the first derivative of the photoemission delay. If the photoemssion delay represents some orientation and emission-angle average of the group-delay of the photoelectron wavepacket [1], then the quantity shown in this panel represents the group-delay dispersion (GDD), or chirp, of the average wavepacket. For electron kinetic energies above 5 eV, the 7-channel MCSCI results shows good agreement with the measurement. There is a notable exception above 10 eV, which suggests there are additional ionization channels which are not captured in the theory.

Fig. 4 (b) shows the integral of the photoemission delay. This can be directly compared to the orientation- and emission-angle-averaged phase of the dipole matrix element. Again the 7-channel MCSCI result shows excellent agreement with the measurement. We can use this phase to approximate the orientation- and emission-angle-averaged electronic wavepacket. This wavepacket can be visualized with the Wigner quasi-probability distribution shown in Fig. 4 (e), which is a joint time-frequency representation of the ~~photoionizied~~ photoionized electron. The marginal (or projection) of the Wigner distribution along the energy-axis, shown in Fig. 4 (c), gives the time-dependent probability ($|\psi(t)|^2$, black). The spectral amplitude of the wavepacket is taken from the time-axis marginal and is shown as an inset in panel (c). We compare to the case of ~~an atomic reference~~ a reference pure Coulomb potential (Figure 4 (d) and dashed brown curve in panel (c)). The molecular potential creates an asymmetry in the electronic wavepacket with a sharp rising edge and an extended tail. The Wigner distribution shows us that this extended tail comes from the low energy electrons which are significantly delayed by the molecular potential (in contrast to ~~an atomic~~ a pure Coulomb reference). The Wigner distribution has additional structure near 7 eV and 13 eV, where the quasi-probability is extended along the time-axis. From the MCSCI theory we have identified the 7 eV structure as originating from the combination of a shape resonance and additional autoionizing structures. We postulate that the temporally-elongated feature at 13 eV likely originates from autoionization *via* ~~an~~ additional channels not considered in our current model. The additional analysis, afforded by the density of measurements, provides greater discernment of the theoretical predictions, and offers deeper insight into the scattering and re-shaping of the outgoing electron due to the molecular potential.

There is an additional consideration in K-shell photoionization close to the ionization threshold. Unlike in valence ionization, the core-ionized system produced by x-ray photoionization is highly unstable and (in the case of low-Z systems) will decay within several femtoseconds *via* the process of Auger-Meitner decay. The core vacancy is filled by a valence electron, and the resultant excess energy in the system is released as a high kinetic energy electron. When the K-shell photoelectron is very slow it will be overtaken by the Auger-Meitner electron, which results in a change in the effective ionic potential in which that photoelectron is propagating. The loss in screening results in an additional delay for the photoelectron, which we account for using the

classical model of Russek and Mehlhorn [43]. We find that a complete description of x-ray photoemission delays also requires accounting for post-collision interaction following the ultrafast Auger-Meitner decay in the core-ionized system. The method to ~~account for~~ calculate the additional delay induced by this post-collision interaction (PCI) is described in the ~~SI, and the appropriate correction has been made to the curves shownin Fig. 3.~~ Supplementary Information. The value of this delay is plotted in the lower panel of Fig. 3 ('PCI delay', dotted black line) and has been included in the calculated delay for all the models shown.

We note several additional effects not included in our present modeling which may contribute to the measured delay. The separability of the CLC contribution and photoionization delay is known to break down at low kinetic energies [18], and can be particularly complex in the case of a structured continuum, when the dressing laser field can interact with the bound part of a resonance [44]. Dynamical effects arising from electron-nuclear coupling can also affect the photoionization delay in molecular systems [22, 45–48].

Conclusion

In this work, we have demonstrated the measurement of attosecond photoemission delays at x-ray wavelengths. This measurement was achieved using the experimental technique of attosecond angular streaking to probe the photoemission delay from different core-level orbitals in a molecular system. We used attosecond x-ray pulses from an x-ray free electron laser, which has continuous wavelength tunability across the entire soft x-ray regime. This unique feature of an attosecond XFEL allows us to probe the photoemission delay across the entire ~~NEXAFS~~ x-ray near-edge spectral region. X-ray induced photoelectron emission delays uniquely map the electronic environment of a molecule. We measure an increase in the photoemission delay that we assign to the transient trapping of an ionized electron by the molecular potential very close to the oxygen K-shell threshold, a so-called shape resonance. We also find that the x-ray photoemission delay is highly sensitive to electron correlation effects: our theoretical description requires the inclusion of orbital relaxation and channel coupling in the final ionized state to explain the sizeable delay in the measurement. In addition, the post-collision interaction between the outgoing photoelectron and the subsequent Auger-Meitner electron from the decay of the core-ionized state induces an additional increase to the photoemission delay measurement. This effect has ~~yet to be observed in photoemission studies~~not been observed previously, because only core-level ionization produces fast AM electrons. Our work provides a new experimental probe of electron correlation effects in quantum systems; by directly accessing the multi-electron dynamics of a fundamental process, the x-ray photoelectric effect, on its natural attosecond timescale. Providing detailed understanding of electrons in the attosecond regime allows the determination of the properties of matter.

Acknowledgements:

Use of the Linac Coherent Light Source (LCLS), SLAC National Accelerator Laboratory, is supported by the U.S. Department of Energy (DOE), Office of Science, Office of Basic Energy Sciences (BES) under Contract No. DE-AC02-76SF00515. This work was

supported primarily by the AMO Physics Program, Chemical Sciences, Geosciences and Biosciences Division (CSGB), BES, DOE. A.M. J.D., and Z.G. acknowledge support from the Accelerator and Detector Research Program of the Department of Energy, Basic Energy Sciences division. A.L. and L.O. were supported by DOE Investigator-Initiated Research grant, Award ID DE-SC0022093, of CSGB, BES, DOE. N.B. acknowledges support from Chemical Sciences, Geosciences and Biosciences Division (CSGB), BES, DOE under award No DE-SC0012376. P.R. and M.F.K. acknowledge support by the German Research Foundation through LMUexcellent. I.I. acknowledges support from the Institute for Basic Science grant (IBS-R012-D1).

Data Availability

The data supporting the findings of this study are available from the corresponding authors upon request.

Methods:

~~*Generating sub-femtosecond*~~ *Sub-femtosecond X-ray pulses:*

The attosecond x-ray pulses were produced using the method described in Ref. [24]. The present experiment was part of a series of beamtimes at the LCLS, and just prior to these measurements, we collected the data used to measure the time-domain profile of the attosecond x-ray pulses. These previous results were published in reference [24], in which we measured a median pulse duration (FWHM) of 480 as at 570 eV. We used the same FEL configuration to produce the pulses in the present work, and therefore the distribution of pulse durations will be the same.

Streaking laser setup:

X-rays generated in the undulators are focused with a pair of Kirkpatrick–Baez mirrors to a spot size of ~ 55 μm diameter (FWHM). The streaking laser pulse is generated using an optical parametric amplifier (TOPAS-HE, Light Conversion) pumped by the titanium-doped sapphire laser system (10 mJ, ~ 40 fs, 800 nm, 120 Hz) synchronized to the accelerator. The OPA is tuned to 2400 nm with a pulse energy of 200 μJ. A quarter-wave plate (Thorlabs AQWP05M-1600) is used to produce circularly polarized laser pulses, which are then focused with a 750 mm focal length CaF_2 lens. The streaking laser field is combined with the XFEL beam using a silver mirror with a 2-mm-diameter drilled hole, and both pulses come to a common focus in the interaction region of a coaxial velocity map imaging apparatus [33]. The laser is focused to a diameter of ~ 110 μm.

Partial Covariance Analysis:

We calculate the partial correlation maps shown in Fig. 2 **b** by calculating the partial correlation coefficient between the radially integrated intensities I_N and I_O at each pair of angles θ_N, θ_O, according to [49]:

$$\rho(\theta_N,\theta_O) = \frac{\mathrm{PCov}\left(I_N(\theta_N), I_O(\theta_O); P\right)}{\sqrt{\mathrm{PCov}\left(I_N(\theta_N), I_N(\theta_N); P\right)\mathrm{PCov}\left(I_O(\theta_O), I_O(\theta_O); P\right)}}, \tag{3}$$

where

$$\mathrm{PCov}\,(X,Y;I) = \mathrm{Cov}\,(X,Y) - \frac{\mathrm{Cov}\,(X,I)\,\mathrm{Cov}\,(I,Y)}{\mathrm{Var}\,(I)}, \tag{4}$$

and

$$\mathrm{Cov}\,(X,Y) = \langle XY\rangle - \langle X\rangle\langle Y\rangle. \tag{5}$$

The angular brackets denote the average across multiple XFEL shots. The partial correlation controls for the single-shot x-ray pulse intensity (P), which is an inherently fluctuating value for SASE FELs. From the partial correlation maps, we identify the offset of the maximum from the diagonal line described by $\theta_N = \theta_O$, in those regions of the detector where the radial gradient of the measured momentum distribution dominates, i.e. the highlighted regions in Fig. 2 (c). As described in section 4 of the supporting material, this offset corresponds to the angular difference between the momentum shift of the two photoemission features. We identify the offset by transforming the axes to $(\theta_O, \pi + \theta_O - \theta_N)$ and averaging across θ_N to produce a one-dimensional trace. The peak of this trace corresponds to the difference in the angular direction of the momentum shift imparted on the two photolines by the streaking laser. We identify the peak by finding the root of the derivative of the polynomial which fits this trace ±40 ° about the maximum. The quoted error bar is the uncertainty in this root due to the uncertainty in the fit coefficients for the polynomial.

The method of modeling of the photoionization matrix element within the Hartree Fock framework using the aug-cc-pVQZ basis set [50] is described in detail in references [51] and [37]. The MCSCI calculations are performed according to the method described in [40]. Further information on these calculations is provided in the supporting material. The molecular-frame photoionization dipole moment is expanded is a spherical harmonic basis:

$$\left\langle \psi^{(-)}_{i,\vec{k}} | \vec{r} | \Psi_0 \right\rangle = \sum_{l,m\mu} I^{(i)}_{lm\mu}(k) Y_{l,m}(\hat{k}) \mathcal{D}^{(1)}_{\mu 0}(\hat{R}), \tag{6}$$

where the subscript i refers to the photoionization channel, $\vec{k}$ is the momentum of the ~~photoionizied~~ photoionized electron, Ψ_0 is the ground state of the molecular system, $Y_{l,m}$ is the spherical harmonic, and $\mathcal{D}^{(l)}_{m_1,m_2}$ is the Wigner-D matrix which rotates the laboratory frame into the molecular frame, $\hat{R}$. The photoemission delay is calculated from $I^{(i)}_{lm\mu}(k)$ according to [38]:

$$\tau = \int d\hat{k} \int d\hat{R}\, \frac{|\sum_{l,m} I_{\hat{R},l,m} Y_{l,m}(\hat{k})|^2}{\sum_{l,m} |I_{\hat{R},l,m}|^2} \times \frac{\partial}{\partial E} \left(\sum_{l,m} I_{\hat{R},l,m} Y_{l,m}(\hat{k}) \right), \tag{7}$$

where the orientation- and emission-angle-delay is averaged over over all molecular orientations $\vec{R}$ and all outgoing electron directions $\vec{k}$ weighted by the relative cross-section.

References

[1] Schultze, M., Fieß, M., Karpowicz, N., Gagnon, J., Korbman, M., Hofstetter, M., Neppl, S., Cavalieri, A.L., Komninos, Y., Mercouris, T., Nicolaides, C.A., Pazourek, R., Nagele, S., Feist, J., Burgdörfer, J., Azzeer, A.M., Ernstorfer, R., Kienberger, R., Kleineberg, U., Goulielmakis, E., Krausz, F., Yakovlev, V.S.: Delay in Photoemission. Science **328**(5986), 1658–1662 (2010) https://doi.org/10.1126/science.1189401 . Accessed 2018-02-21

[2] The Nobel Committee for Physics: Scientific Background to the Nobel Prize in Physics 2023 (2023). https://www.nobelprize.org/uploads/2023/10/advanced-physicsprize2023.pdf

[3] Ossiander, M., Siegrist, F., Shirvanyan, V., Pazourek, R., Sommer, A., Latka, T., Guggenmos, A., Nagele, S., Feist, J., Burgdörfer, J., Kienberger, R., Schultze, M.: Attosecond correlation dynamics. Nature Physics **13**(3), 280–285 (2017) https://doi.org/10.1038/nphys3941 . Accessed 2019-06-19

[4] Isinger, M., Squibb, R.J., Busto, D., Zhong, S., Harth, A., Kroon, D., Nandi, S., Arnold, C.L., Miranda, M., Dahlström, J.M., Lindroth, E., Feifel, R., Gisselbrecht, M., L'Huillier, A.: Photoionization in the time and frequency domain. Science **358**(6365), 893–896 (2017) https://doi.org/10.1126/science.aao7043 . Accessed 2019-09-17

[5] Månsson, E.P., Guénot, D., Arnold, C.L., Kroon, D., Kasper, S., Dahlström, J.M., Lindroth, E., Kheifets, A.S., L'Huillier, A., Sorensen, S.L., Gisselbrecht, M.: Double ionization probed on the attosecond timescale. Nature Physics **10**(3), 207–211 (2014) https://doi.org/10.1038/nphys2880 . Accessed 2018-06-05

[6] Biswas, S., Förg, B., Ortmann, L., Schötz, J., Schweinberger, W., Zimmermann, T., Pi, L., Baykusheva, D., Masood, H.A., Liontos, I., Kamal, A.M., Kling, N.G., Alharbi, A.F., Alharbi, M., Azzeer, A.M., Hartmann, G., Wörner, H.J., Landsman, A.S., Kling, M.F.: Probing molecular environment through photoemission delays. Nature Physics, 1–6 (2020) https://doi.org/10.1038/s41567-020-0887-8 . Publisher: Nature Publishing Group. Accessed 2020-05-12

[7] Haessler, S., Fabre, B., Higuet, J., Caillat, J., Ruchon, T., Breger, P., Carré, B., Constant, E., Maquet, A., Mével, E., Salières, P., Taïeb, R., Mairesse, Y.: Phase-resolved attosecond near-threshold photoionization of molecular nitrogen. Physical Review A **80**(1), 011404 (2009) https://doi.org/10.1103/PhysRevA.80.011404 . Accessed 2017-04-12

[8] Gruson, V., Barreau, L., Jiménez-Galan, , Risoud, F., Caillat, J., Maquet, A., Carré, B., Lepetit, F., Hergott, J.-F., Ruchon, T., Argenti, L., Taïeb, R., Martín, F., Salières, P.: Attosecond dynamics through a Fano resonance: Monitoring the birth of a photoelectron. Science **354**(6313), 734–738 (2016) https://doi.org/10.1126/science.aah5188 . Accessed 2016-12-29

[9] Kotur, M., Guénot, D., Jiménez-Galán, , Kroon, D., Larsen, E.W., Louisy, M., Bengtsson, S., Miranda, M., Mauritsson, J., Arnold, C.L., Canton, S.E., Gisselbrecht, M., Carette, T., Dahlström, J.M., Lindroth, E., Maquet, A., Argenti, L., Martín, F., L'Huillier, A.: Spectral phase measurement of a Fano resonance using tunable attosecond pulses. Nature Communications **7**, 10566 (2016) https://doi.org/10.1038/ncomms10566 . Accessed 2018-02-14

[10] Kamalov, A., Wang, A.L., Bucksbaum, P.H., Haxton, D.J., Cryan, J.P.: Electron correlation effects in attosecond photoionization of ${\mathrm{CO}}_{2}$. Physical Review A **102**(2), 023118 (2020) https://doi.org/10.1103/PhysRevA.102.023118 . Publisher: American Physical Society. Accessed 2020-10-20

[11] Cirelli, C., Marante, C., Heuser, S., Petersson, C.L.M., Galán, J., Argenti, L., Zhong, S., Busto, D., Isinger, M., Nandi, S., Maclot, S., Rading, L., Johnsson, P., Gisselbrecht, M., Lucchini, M., Gallmann, L., Dahlström, J.M., Lindroth, E., L'Huillier, A., Martín, F., Keller, U.: Anisotropic photoemission time delays close to a Fano resonance. Nature Communications **9**(1), 955 (2018) https://doi.org/10.1038/s41467-018-03009-1 . Accessed 2018-06-26

[12] Peschel, J., Busto, D., Plach, M., Bertolino, M., Hoflund, M., Maclot, S., Vinbladh, J., Wikmark, H., Zapata, F., Lindroth, E., Gisselbrecht, M., Dahlström, J.M., L'Huillier, A., Eng-Johnsson, P.: Attosecond dynamics of multi-channel single photon ionization. Nature Communications **13**(1), 5205 (2022) https://doi.org/10.1038/s41467-022-32780-5 . Number: 1 Publisher: Nature Publishing Group. Accessed 2022-11-17

[13] Pazourek, R., Nagele, S., Burgdörfer, J.: Attosecond chronoscopy of photoemission. Reviews of Modern Physics **87**(3), 765–802 (2015) https://doi.org/10.1103/RevModPhys.87.765

[14] Véniard, V., Taïeb, R., Maquet, A.: Phase dependence of (n+ 1)-color (n¿ 1) ir-uv photoionization of atoms with higher harmonics. Physical Review A **54**(1), 721 (1996)

[15] Paul, P.M., Toma, E.S., Breger, P., Mullot, G., Augé, F., Balcou, P., Muller, H.G., Agostini, P.: Observation of a Train of Attosecond Pulses from High Harmonic Generation. Science **292**(5522), 1689–1692 (2001) https://doi.org/10.1126/science.1059413 . Accessed 2017-07-26

[16] Klünder, K., Dahlström, J.M., Gisselbrecht, M., Fordell, T., Swoboda, M., Guénot, D., Johnsson, P., Caillat, J., Mauritsson, J., Maquet, A., Taïeb, R., L'Huillier, A.: Probing Single-Photon Ionization on the Attosecond Time Scale. Physical Review Letters **106**(14), 143002 (2011) https://doi.org/10.1103/PhysRevLett.106.143002

[17] Kienberger, R., Goulielmakis, E., Uiberacker, M., Baltuska, A., Yakovlev, V., Bammer, F., Scrinzi, A., Westerwalbesloh, T., Kleineberg, U., Heinzmann, U.,

Drescher, M., Krausz, F.: Atomic transient recorder. Nature **427**(6977), 817–821 (2004) https://doi.org/10.1038/nature02277 . Accessed 2017-04-01

[18] Dahlström, J.M., Guénot, D., Klünder, K., Gisselbrecht, M., Mauritsson, J., L'Huillier, A., Maquet, A., Taïeb, R.: Theory of attosecond delays in laser-assisted photoionization. Chemical Physics **414**, 53–64 (2013) https://doi.org/10.1016/j.chemphys.2012.01.017 . Accessed 2017-03-23

[19] Zipp, L.J., Natan, A., Bucksbaum, P.H.: Probing electron delays in above-threshold ionization. Optica **1**(6), 361–364 (2014) https://doi.org/10.1364/OPTICA.1.000361 . Publisher: Optical Society of America. Accessed 2021-05-26

[20] Vos, J., Cattaneo, L., Patchkovskii, S., Zimmermann, T., Cirelli, C., Lucchini, M., Kheifets, A., Landsman, A.S., Keller, U.: Orientation-dependent stereo Wigner time delay and electron localization in a small molecule. Science **360**(6395), 1326–1330 (2018) https://doi.org/10.1126/science.aao4731 . Accessed 2018-06-26

[21] Huppert, M., Jordan, I., Baykusheva, D., Conta, A., Wörner, H.J.: Attosecond Delays in Molecular Photoionization. Physical Review Letters **117**(9), 093001 (2016) https://doi.org/10.1103/PhysRevLett.117.093001 . Accessed 2017-03-20

[22] Nandi, S., Plésiat, E., Zhong, S., Palacios, A., Busto, D., Isinger, M., Neoričić, L., Arnold, C.L., Squibb, R.J., Feifel, R., Decleva, P., L'Huillier, A., Martín, F., Gisselbrecht, M.: Attosecond timing of electron emission from a molecular shape resonance. Science Advances **6**(31), 7762 (2020) https://doi.org/10.1126/sciadv.aba7762 . Publisher: American Association for the Advancement of Science Section: Research Article. Accessed 2020-08-13

[23] Heck, S., Baykusheva, D., Han, M., Ji, J.-B., Perry, C., Gong, X., Wörner, H.J.: Attosecond interferometry of shape resonances in the recoil frame of CF4. Science Advances **7**(49), 8121 (2021) https://doi.org/10.1126/sciadv.abj8121 . Publisher: American Association for the Advancement of Science. Accessed 2023-12-30

[24] Duris, J., Li, S., Driver, T., Champenois, E.G., MacArthur, J.P., Lutman, A.A., Zhang, Z., Rosenberger, P., Aldrich, J.W., Coffee, R., Coslovich, G., Decker, F.-J., Glownia, J.M., Hartmann, G., Helml, W., Kamalov, A., Knurr, J., Krzywinski, J., Lin, M.-F., Marangos, J.P., Nantel, M., Natan, A., O'Neal, J.T., Shivaram, N., Walter, P., Wang, A.L., Welch, J.J., Wolf, T.J.A., Xu, J.Z., Kling, M.F., Bucksbaum, P.H., Zholents, A., Huang, Z., Cryan, J.P., Marinelli, A.: Tunable isolated attosecond X-ray pulses with gigawatt peak power from a free-electron laser. Nature Photonics **14**(1), 30–36 (2020) https://doi.org/10.1038/s41566-019-0549-5 . Number: 1 Publisher: Nature Publishing Group. Accessed 2020-10-20

[25] Itatani, J., Quéré, F., Yudin, G.L., Ivanov, M.Y., Krausz, F., Corkum, P.B.: Attosecond Streak Camera. Physical Review Letters **88**(17), 173903 (2002) https://doi.org/10.1103/PhysRevLett.88.173903 . Accessed 2016-12-01

[26] Hartmann, N., Hartmann, G., Heider, R., Wagner, M.S., Ilchen, M., Buck, J., Lindahl, A.O., Benko, C., Grünert, J., Krzywinski, J., Liu, J., Lutman, A.A., Marinelli, A., Maxwell, T., Miahnahri, A.A., Moeller, S.P., Planas, M., Robinson, J., Kazansky, A.K., Kabachnik, N.M., Viefhaus, J., Feurer, T., Kienberger, R., Coffee, R.N., Helml, W.: Attosecond time–energy structure of X-ray free-electron laser pulses. Nature Photonics **12**(4), 215–220 (2018) https://doi.org/10.1038/s41566-018-0107-6 . Accessed 2018-08-30

[27] Eckle, P., Pfeiffer, A.N., Cirelli, C., Staudte, A., Dörner, R., Muller, H.G., Büttiker, M., Keller, U.: Attosecond Ionization and Tunneling Delay Time Measurements in Helium. Science **322**(5907), 1525–1529 (2008) https://doi.org/10.1126/science.1163439 . Accessed 2018-08-07

[28] Li, S., Driver, T., Rosenberger, P., Champenois, E.G., Duris, J., Al-Haddad, A., Averbukh, V., Barnard, J.C.T., Berrah, N., Bostedt, C., Bucksbaum, P.H., Coffee, R.N., DiMauro, L.F., Fang, L., Garratt, D., Gatton, A., Guo, Z., Hartmann, G., Haxton, D., Helml, W., Huang, Z., LaForge, A.C., Kamalov, A., Knurr, J., Lin, M.-F., Lutman, A.A., MacArthur, J.P., Marangos, J.P., Nantel, M., Natan, A., Obaid, R., O'Neal, J.T., Shivaram, N.H., Schori, A., Walter, P., Wang, A.L., Wolf, T.J.A., Zhang, Z., Kling, M.F., Marinelli, A., Cryan, J.P.: Attosecond coherent electron motion in Auger-Meitner decay. Science (2022) https://doi.org/10.1126/science.abj2096 . Publisher: American Association for the Advancement of Science. Accessed 2022-01-25

[29] Tsuchiya, Y.: Advances in streak camera instrumentation for the study of biological and physical processes. IEEE Journal of Quantum Electronics **20**(12), 1516–1528 (1984) https://doi.org/10.1109/JQE.1984.1072316 . Conference Name: IEEE Journal of Quantum Electronics

[30] Bradley, D., Liddy, B., Sleat, W.: Direct linear measurement of ultrashort light pulses with a picosecond streak camera. Optics Communications **2**(8), 391–395 (1971)

[31] Serov, V.V., Derbov, V.L., Sergeeva, T.A.: Interpretation of time delay in the ionization of two-center systems. Physical Review A **87**(6), 063414 (2013) https://doi.org/10.1103/PhysRevA.87.063414 . Accessed 2019-04-09

[32] Zholents, A.A.: Method of an enhanced self-amplified spontaneous emission for x-ray free electron lasers. Physical Review Special Topics - Accelerators and Beams **8**(4), 040701 (2005) https://doi.org/10.1103/PhysRevSTAB.8.040701 . Accessed 2016-10-03

[33] Li, S., Champenois, E.G., Coffee, R., Guo, Z., Hegazy, K., Kamalov, A., Natan, A., O'Neal, J., Osipov, T., Owens, M., Ray, D., Rich, D., Walter, P., Marinelli, A., Cryan, J.P.: A co-axial velocity map imaging spectrometer for electrons. AIP Advances **8**(11), 115308 (2018) https://doi.org/10.1063/1.5046192 . Publisher: American Institute of Physics. Accessed 2020-10-20

[34] Glownia, J.M., Cryan, J., Andreasson, J., Belkacem, A., Berrah, N., Blaga, C.I., Bostedt, C., Bozek, J., DiMauro, L.F., Fang, L., Frisch, J., Gessner, O., Gühr, M., Hajdu, J., Hertlein, M.P., Hoener, M., Huang, G., Kornilov, O., Marangos, J.P., March, A.M., McFarland, B.K., Merdji, H., Petrovic, V.S., Raman, C., Ray, D., Reis, D.A., Trigo, M., White, J.L., White, W., Wilcox, R., Young, L., Coffee, R.N., Bucksbaum, P.H.: Time-resolved pump-probe experiments at the LCLS. Optics Express **18**(17), 17620–17630 (2010) https://doi.org/10.1364/OE.18.017620 . Accessed 2018-12-12

[35] Kosugi, N., Adachi, J.-i., Shigemasa, E., Yagishita, A.: High-resolution and symmetry-resolved N and O K-edge absorption spectra of NO. The Journal of Chemical Physics **97**(12), 8842–8849 (1992) https://doi.org/10.1063/1.463359 . Accessed 2017-03-23

[36] Rüdel, A., Hergenhahn, U., Maier, K., Rennie, E.E., Kugeler, O., Viefhaus, J., Lin, P., Lucchese, R.R., Bradshaw, A.M.: Exchange interaction effects in NO core-level photoionization cross-sections. New Journal of Physics **7**, 189–189 (2005) https://doi.org/10.1088/1367-2630/7/1/189 . Publisher: IOP Publishing. Accessed 2022-03-07

[37] Mountney, M.E., Driver, T.C., Marinelli, A., Kling, M.F., Cryan, J.P., Emmanouilidou, A.: Streaking single-electron ionization in open-shell molecules driven by x-ray pulses. Physical Review A **107**(6), 063111 (2023) https://doi.org/10.1103/PhysRevA.107.063111 . Publisher: American Physical Society. Accessed 2023-07-25

[38] Baykusheva, D., Wörner, H.J.: Theory of attosecond delays in molecular photoionization. The Journal of Chemical Physics **146**(12), 124306 (2017) https://doi.org/10.1063/1.4977933 . Accessed 2018-02-21

[39] Piancastelli, M.N.: The neverending story of shape resonances. Journal of Electron Spectroscopy and Related Phenomena **100**(1), 167–190 (1999) https://doi.org/10.1016/S0368-2048(99)00046-8 . Accessed 2020-01-23

[40] Li, W.B., Montuoro, R., Houver, J.C., Journel, L., Haouas, A., Simon, M., Lucchese, R.R., Dowek, D.: Photoemission in the NO molecular frame induced by soft-x-ray elliptically polarized light above the $\mathrm{N}{(1s)}ˆ{\ensuremath{-}1}$ and $\mathrm{O}{(1s)}ˆ{\ensuremath{-}1}$ ionization thresholds. Physical Review A **75**(5), 052718 (2007) https://doi.org/10.1103/PhysRevA.75.052718 . Publisher: American Physical Society. Accessed 2022-04-25

[41] Breidbach, J., Cederbaum, L.S.: Universal Attosecond Response to the Removal of an Electron. Physical Review Letters **94**(3), 033901 (2005) https://doi.org/10.1103/PhysRevLett.94.033901 . Accessed 2015-08-12

[42] Lin, P., Lucchese, R.R.: Theoretical studies of core excitation and ionization in molecular systems. Journal of Synchrotron Radiation **8**(2), 150–153 (2001)

https://doi.org/10.1107/S0909049500014308 . Publisher: International Union of Crystallography. Accessed 2023-07-25

[43] Russek, A., Mehlhorn, W.: Post-collision interaction and the Auger lineshape. Journal of Physics B: Atomic and Molecular Physics **19**(6), 911 (1986) https://doi.org/10.1088/0022-3700/19/6/013 . Accessed 2023-04-19

[44] Argenti, L., Jiménez-Galán, , Caillat, J., Taïeb, R., Maquet, A., Martín, F.: Control of photoemission delay in resonant two-photon transitions. Physical Review A **95**(4), 043426 (2017) https://doi.org/10.1103/PhysRevA.95.043426 . Accessed 2019-08-06

[45] Cattaneo, L., Vos, J., Bello, R.Y., Palacios, A., Heuser, S., Pedrelli, L., Lucchini, M., Cirelli, C., Martín, F., Keller, U.: Attosecond coupled electron and nuclear dynamics in dissociative ionization of H 2. Nature Physics, 1 (2018) https://doi.org/10.1038/s41567-018-0103-2 . Accessed 2018-04-25

[46] Wang, A.L., Serov, V.V., Kamalov, A., Bucksbaum, P.H., Kheifets, A., Cryan, J.P.: Role of nuclear-electronic coupling in attosecond photoionization of ${\mathrm{H}}_{2}$. Physical Review A **104**(6), 063119 (2021) https://doi.org/10.1103/PhysRevA.104.063119 . Publisher: American Physical Society. Accessed 2022-10-05

[47] Borràs, V.J., González-Vázquez, J., Argenti, L., Martín, F.: Attosecond photoionization delays in the vicinity of molecular Feshbach resonances. Science Advances **9**(15), 3855 (2023) https://doi.org/10.1126/sciadv.ade3855 . Publisher: American Association for the Advancement of Science. Accessed 2024-04-01

[48] Hammerland, D., Berglitsch, T., Zhang, P., Luu, T.T., Ueda, K., Lucchese, R.R., Wörner, H.J.: Bond-length dependence of attosecond ionization delays in O2 arising from electron correlation to a shape resonance. Science Advances **10**(13), 3810 (2024) https://doi.org/10.1126/sciadv.adl3810 . Publisher: American Association for the Advancement of Science. Accessed 2024-04-01

[49] Johnson, R.A., Wichern, D.W.: In: Applied Multivariate Statistical Analysis, 6th edn., pp. 409–410. Pearson, Upper Saddle River, NJ (2007)

[50] Dunning Jr, T.H.: Gaussian basis sets for use in correlated molecular calculations. i. the atoms boron through neon and hydrogen. The Journal of chemical physics **90**(2), 1007–1023 (1989)

[51] Banks, H., Little, D., Tennyson, J., Emmanouilidou, A.: Interaction of molecular nitrogen with free-electron-laser radiation. Physical Chemistry Chemical Physics **19**(30), 19794–19806 (2017)